Available online at www.sciencedirect.com

jmr&t Journal of Materials Research and Technology

www.jmrt.com.br

Original Article

Binary modelling the milling of UG2 ore using a matrix approach

Méschac-Bill Kime[a,*], *Michael H. Moys*[b]

[a] *Department of Metallurgy, University of Johannesburg, Johannesburg, South Africa*

[b] *School of Chemical and Metallurgical Engineering, University of the Witwatersrand, Johannesburg, South Africa*

ARTICLE INFO

Article history:
Received 9 June 2015
Accepted 11 October 2016
Available online 25 November 2016

Keywords:
Grinding circuit
Ball mill
Hydrocyclone
Vibrating screen
Population balance modelling
Matrix approach
UG2 ore
Chromite

ABSTRACT

The study reports a binary matrix modelling and simulation studies to improve the performance of the secondary grinding circuit of UG2 ores. The model developed was intended to help searching for optimal operating conditions of the secondary milling circuit so that the platinum group element (PGE) recovery is increased while reducing Cr_2O_3 entrainment in the subsequent flotation stage. A series of laboratory batch-scale tests was carried out in order to estimate the milling kinetics parameters of the chromite and non-chromite components. Finally, two alternatives circuit configurations for a better performance were evaluated using simulations. The optimal design consisted of a conventional ball mill in closed circuit with a hydrocyclone to separate the milling product into lights (non-chromite-rich) and heavies (chromite-rich) fractions followed by a vibrating screen to de-slime the cyclone underflow before it is returned to the mill for further grinding.

1. Introduction

Simulations of grinding circuits using mathematical models are increasingly used in comminution because of their low cost and their ability to consider many variables simultaneously [1,2]. Results from simulations can provide useful information on the effects of proposed changes on the circuit performance in terms of size distribution and material composition under various operating conditions. The size distribution and composition of materials in grinding circuits are often quantified by population balance models, more appropriately called size-mass balance models [3]. Many of these models are very complex that their simplified approaches are preferred to describe the steady-state and dynamic performance of grinding mills [4–8]. The aura of these models lies in that they are powerful frameworks that can be used to maintain the mass integrity and describe the output of equipment [7,9]. Their Achilles' heel is that they are limited to describing the behaviour of the size distribution and composition of material inside the mill in terms of input and output. They are not also suitable, in general to combine both size reduction

* *Corresponding author.*
E-mail: mbkime@uj.ac.za (M.B. Kime).

http://dx.doi.org/10.1016/j.jmrt.2016.10.001

model and liberation model in the same model framework. Further, population balance models do not describe in a very comprehensive way individual milling kinetics behaviours of multi-component ores. Some examples on the milling kinetics modelling of multi-component ores simulated using simplified population models are given hereinafter. Finch and Ramirez-Castro [5] used a simplified population balance model, referred to as the cumulative breakage rate function to describe the individual mineral grinding kinetics behaviours of some ores processed at Pine Point mines concentrator. A similar approach was later extended, by Laplante et al. [6] to describe the grinding mill circuit of multiple classes of composite particles. More recently, Hinde and Kalala [8] adopted the same approach to reconcile the behaviour of chromite and silicates in the closed circuit milling of UG2 platinum ores. A simplistic way of representing grinding population balances is by use of matrices [1]. The transformation matrix approach can be very useful in describing individual milling kinetics parameters (Selection, Breakage, Discharge and Partition curve Functions) of multi-component ores during grinding circuit simulations. The matrix modelling approach was successfully used by Choi et al. [10] to estimate the individual milling parameters of ZnS and gangue of a sphalerite ore. A similar approach was used by Herbst et al. [11] to develop a multi-component-multi-size liberation model of a copper ore.

The aim of the study was to develop a binary matrix model that adequately describes the grinding kinetics behaviour of chromite and non-chromite components during ball milling in a closed circuit with a hydrocyclone and a screen, and to investigate the effects of the proposed circuit configuration on the minimization of chromite content in downstream processes using simulations.

2. Contextualization

Platinum concentrators in South Africa experience significant losses of valuable platinum group metals (PGM) in their secondary milling circuits due to insufficient liberation of platinum-bearing minerals. In fact, the interlocked texture between chromite and the valuable minerals predisposes the PGM ores to an inefficient froth flotation. Studies on the froth flotation of PGM ores abound (Mailula et al. [12], Hay [13], Hay and Roy [14]) and highlighted the problem brought by a high proportion of chromite in the PGM concentrates. Entrainment mechanism of fine chromite has been recognized to be the main responsible for the contamination of the PGM concentrates. The problem of chromite in PGM concentrates is very critical. Chromite belongs to the spinel group which forms stable compounds at temperatures approaching 2000 °C [15]. A high chromite content in the concentrate impacts negatively on the smelting efficiency. For this reason, the chromite level in the final concentrate has to be kept as low as possible. PGMs in the UG2 are known to be tiny inclusions of an average size of 2–4 μm and maximum size of 25 μm in the PGM ores [16]. This requires a very fine grinding to liberate all the PGMs locked in the silicates, which would lead consequently to the chromite being ground even finer. The current standard circuit design to concentrate PGMs from the UG2 ore consists of a mill-float/mill-float approach designated under the acronym MF2. The motivation behind this approach is to perform a first flotation while keeping chromite as coarse as possible. The tailings from the primary flotation are thickened and separated in a hydrocyclone, and the hydrocyclone underflow is fed to the secondary open circuit ball mill. The feed to the secondary ball mill usually comprises of large amounts of liberated chromite and silicate-rich particles containing the bulk of the PGMs in a locked state [17,18]. However, the efficiency of secondary grinding of UG2 ore is currently limited by the use of open-circuit grinding in many plants, which is inherently inefficient, due to short-circuiting of coarse particles and possible segregation by gravity in the mill. It should be noted that the use of hydrocyclones results in wasting energy and increasing chromite entrainment whilst not effectively allowing for the grinding of silicates to liberate the PGMs and base metals [18]. The fine chromite present in the underflow stream is sent back to the grinding circuit resulting in over-grinding of barren chromite [19]. Hinde and Kalala [8] conducted optimization tests on secondary milling circuits for UG2 ore and found that through the use of fine screening technology, it was evident that the chromite was effectively liberated and virtually barren of PGM. The majority of the PGMs were associated with and locked in the silicate minerals. Hinde and Kalala [8] also noted that the liberated chromite has a much higher density than the silicates and reports preferentially to the hydrocyclone underflow whereas the lighter silicates containing the locked PGM have a tendency to report to the hydrocyclone overflow and therefore do not undergo secondary milling. This clearly highlights the problem of the inefficiencies in the hydrocyclone circuit. Many attempts have been made over the years to replace hydrocyclones with vibrating screens in UG2 concentrators [8]. Although the energy saving benefit was noted in many cases, the changes were not practical based on current technology. It was noted that a considerable breakthrough was achieved with the introduction of new fine screening technology with the introduction of the Stacksizer by Derrick Corporation in the USA. These screens were non-blinding with high open areas and with a high lifespan as compared with conventional wire mesh screens. This does indicate that using hydrocyclones and screens in closed circuit with ball mills would be a good solution since the separation relies on both particle size and particle density.

3. Theoretical background

3.1. *Breakage and Selection Functions: theoretical background*

The conventional ball mill model is based on the so-called “Modern Theory of Comminution”. In this theory the comminution operation, such as ball milling, is regarded as the sum of many repetitive individual comminution events [20,21] and calls up two probabilistic sets of parameters: the Selection Function S and the Breakage Function B. The former, also called grindability refers to the grinding kinetics of each independent particle. The latter, also called distribution of primary fragments characterizes the size distribution of the resulting fragments following the breakage events.

3.1.1. Selection Function

It is generally accepted that the disappearance rate of particles through milling is directly proportional to the amount of particles present. In other words, the breakage of a given size fraction of material is assumed to follow the first-order law [2]. Although no theory objectively justifies this behaviour so far, this law has proven to be applicable to many materials over a wide range of operation, especially for fine size materials [2,4].

Mathematically, the breakage rate of material, which is in the top size, is given as follows:

$$\frac{dw_i}{dt} = -S_i \cdot w_i(t) \tag{1}$$

The solution of this differential Eq. (1) is

$$\log(w_i(t)) = -\log(w_i(0)) = \frac{S_i t}{2.3} \tag{2}$$

where $w_i(t)$ and $w_i(0)$ are respectively the weight fraction of size i at times t and 0. S_i is the selection function of the size i. The largest size class is class no 1.

In some cases, deviations due to the material characteristics and grinding conditions used from the first-order can occur [22,23]. In order to define the variation of the specific rate of breakage function with the particle size, the following empirical model can be used [4]:

$$S = \frac{a x_i^{\alpha}}{1 + (x_i/\mu)^{\Lambda}} \tag{3}$$

where x_i is the upper limit of the particle size interval under consideration; the model parameters a and μ are mainly functions of the grinding conditions while α and Λ are material properties.

The parameter α is a positive number normally in the range 0.5–1.5. It is mainly characteristic of the material properties and does not vary with mill rotational speed, ball load, ball size or mill hold-up over the normal recommended test ranges [24] for dry milling. The value of a in turn depends on the mill conditions. The denominator term $Q(x_i) = 1/(1 + (x_i/\mu)^{\Lambda})$ is a correction factor. μ defines the particle size at which $Q(x_i) = 0.5$. Λ is an index that shows how rapidly the rate of breakage decreases as the particle size increases. Where all particle sizes fall within the normal breakage range (i.e. particle sizes are substantially finer than the largest particles that the mill can handle): $Q(x_i) = 1$, S is expressed as follows

$$S = a(x_i)^{\alpha} \tag{4}$$

a is a parameter that depends on the milling conditions while α is mainly characteristic of the material properties.

3.1.2. Breakage Function

The primary breakage distribution function $b_{i,j}$ is the sum of the mass fractions of material broken out of size j that is smaller than the upper size of interval i [25].

Mathematically

$$b_{i,j} = \frac{\text{mass of particles broken into size } i \text{ from class } j}{\text{mass of class } j \text{ broken}} \tag{5}$$

The cumulative breakage distribution function $B_{i,j}$ is defined as

$$B_{i,j} = \sum_{k=n}^{i} b_{k,j} \tag{6}$$

The breakage function $B_{i,j}$ can be fitted using the following empirical function [4]

$$B = \phi_j \left(\frac{X_{i-1}}{X_j}\right)^{\gamma} + (1 - \phi_j)\left(\frac{X_{i-1}}{X_j}\right)^{\beta} \tag{7}$$

$$\phi_j = \phi_1 \left(\frac{X_j}{X_1}\right)^{-\delta} \tag{8}$$

where δ, ϕ_j, γ and β are the model parameters that depend on the properties for a given ore. The values of γ are typically found to be between 0.5 and 1.5, while the values of β range from 2.5 to 5. ϕ_j represents the fraction of fines that are produced in a single fracture event.

The B_{ij} values are said to be normalizable if the breakage distribution function is independent of the initial particle size [4]. In other words, the fraction which appears at sizes less than the starting size is independent of the starting size. For normalized B values, $\delta = 0$ and the B_{ij} are superimposed upon each other.

3.2. Classification

The classification can be achieved by means of hydrocyclones and screens. The hydrocyclone model by Plitt [26] and measured partition coefficients were used to describe the hydrocyclone unit. In this model the recovery of the solids to underflow in the size class i (R_{ui}) is expressed as follows

$$R_{ui} = R_f + (1 - R_f) \times \left(1 - e^{-0.693 \times (x_i/x_{50c})^m}\right) \tag{9}$$

where R_f is the water recovery to the underflow (which is assumed to be the same as the recovery of the finest particles), m is a parameter indicating the sharpness of separation and is related to the slope of the R_{ui} curve at the point of inflection, x is the particle size (m).

The effect of particle density on the cut size is given by

$$x_{50c} = k_1 \cdot (\rho_{ore} - \rho_{U/F})^{k_2} \tag{10}$$

where ρ_{ore} is the S.G. of the cyclone feed material. $\rho_{U/F}$ is the S.G. of the liquid phase. It normally takes value around the water density. k_1 and k_2 are dimensionless calibration factors. k_2 takes values between −1 and −0.5.

For the classification by means of a screen, the model by Rogers [27] was considered. This model has been found to be effective for wet screening and has been tested for different material slurries on vibrating screens [28]. The classification function is described by

$$E = \frac{1}{\left(1 + e^{\alpha(1-x^3)/x}\right)} \tag{11}$$

with $x = d_p/d_{50c}$.

Because the short circuit to oversize follows the water split, the actual classification is expressed as follows

$$y = 1 - A + A \times E \tag{12}$$

where A is the water split to undersize. d_{50c} is the cut size. α is the screen efficiency parameter. α takes values between 0.8 and 4.0.

3.3. *Determination of chromite relative mass fractions*

Eq. (13) was used to calculate the relative mass fractions of chromite in different size fractions.

$$C = 100 \times \frac{(1/\rho) - (1/rho_2)}{(1/rho_1) - (1/rho_2)} \tag{13}$$

where C is the size fraction chromite grade; ρ, rho_1 and rho_2 are the S.G. of UG2 ore, chromite and non-chromite, respectively.

ρ was determined from direct measurement of particle size fraction specific density (S.G.), using a gas pycnometer. The remaining variables (rho_1 and rho_2) were estimated using the Excel Subroutine Solver that minimizes the residual error between the measured and predicted chromite grades. The values found for rho_1 and rho_2 were 4.32 and 3.24 respectively. The relative size mass fractions of the non-chromite were obtained by taking the difference between the measured mass fractions and the calculated mass fractions of chromite.

4. Grinding circuit modelling

If one considers particles with size x at time t within a given feed size distribution; we denote their mass fraction as $w(x, t)$. Let one also take a time interval dt small enough to allow only single breakage to occur on a fraction of $w(x, t)$. If the fraction selected for single event breakage per unit time is $S(x)$, then $S(x)\cdot dt$ represents the mass fraction broken after the time interval dt. This mass breaks theoretically into a wide range of children particles the size of which spans from the parent size x down to 0. After time interval dt, the second category of particles is given by $S(x)\cdot dt$ whilst the third necessitates the determination of the mass fraction reporting to $[x, x + dx]$ as a result of breakage of selected particles of initial sizes larger than x. To this end, let us symbolically call y any particle size larger than x (that is, $0 \le y \le x$). It can be seen that selected particles of size y for breakage give birth to particles of sizes spanning from y down to 0. After choosing infinitesimal class intervals $[x, x + dx]$ and $[y, y + dy]$ to represent particles respectively of size x and y, one can determine the fraction of children particles formed after breakage of a unit mass $S(y)$ of parent particles has been selected for breakage from a mass fraction $w(y, t)$. Now, if one chooses $b(x, y)$ to be the mass fraction of children particles from $S(y)\cdot w(y, t)$ reporting to $[x, x + dx]$ after unit time, then for time interval dt, the mass of particles breaking from $[y, y + dy]$ and reporting to $[x, x + dx]$ is given by $b(x, y)\cdot S(y)\cdot w(y, t)\cdot dt$. It is then possible to describe the flow of material in any class interval $[x, x + dx]$ in a batch milling reactor using the following integro-differential equation:

$$\frac{\partial w(x, t)}{\partial t} = -S(x) \cdot w(x, t) + \int_x^{+\infty} b(x, y) \cdot S(y, t) \cdot w(y, t) \cdot dy \tag{14}$$

Eq. (14) is known as the "size-continuous, mass density-size formulation of the population balance model (PBM) for a well-mixed batch grinding process" [29]. We shall see later that the

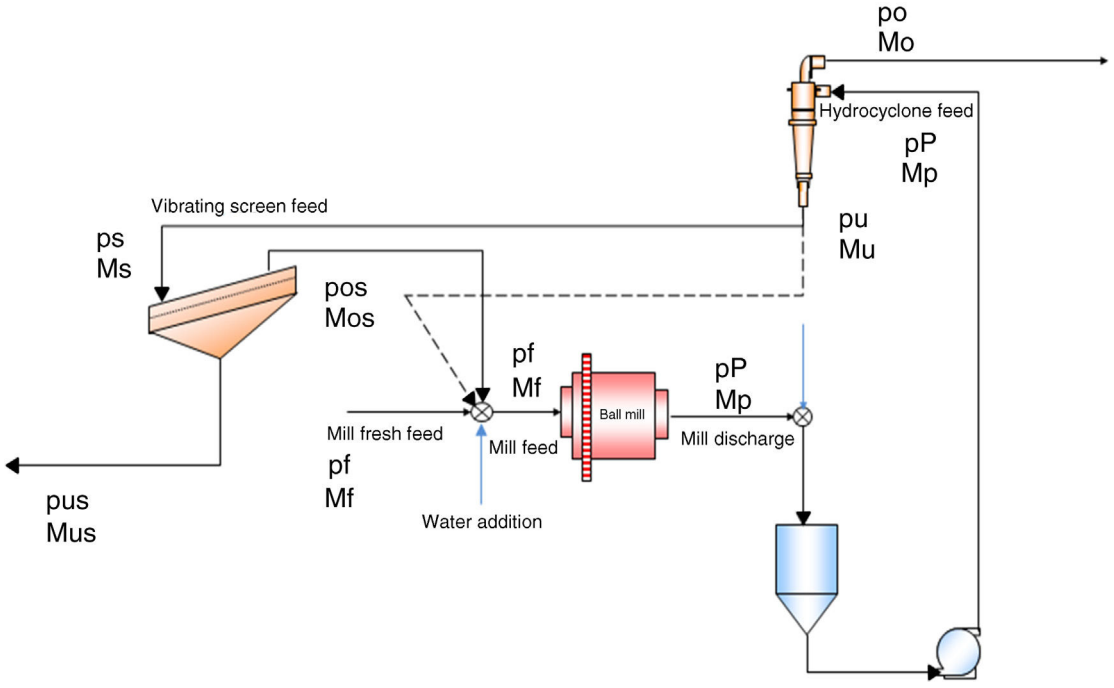

Fig. 1 – Secondary ball milling closed circuit.

size-discrete, time-continuous version of Eq. (14) reduces to Eq. (15) better known as the "batch grinding equation".

$$\frac{dw_i(t)}{dt} = -S_i w_i(t) + \sum_{\substack{j=1 \\ i>1}}^{i-1} b_{i,j} S_j w_j(t), \quad n \geq i \geq j \geq 1 \tag{15}$$

The population balance model can be applied to the milling circuit to show the breakage mechanics and the mass balance around the units involved. Let us consider the closed circuit ball milling design shown in Fig. 1 that consists of a ball mill and classifiers (hydrocyclone and screen). The scripts p_F, p_P, p_o, p_u, p_s, p_{os}, p_{us} are the weight fractions of the incoming and outgoing flows and M_F, M_P, M_o, M_u, M_s, M_{os}, M_{us} are their respective flowrates.

4.1. Mill feed

Using the matrix notation, the mass ball mill feed can be expressed as follows

$$M_{os}\underline{p}_{os} + M_f\underline{p}_f = M_F\underline{p}_F \tag{16}$$

Dividing both sides of Eq. (16) by M_p, one gets

$$\frac{M_{os}}{M_P}\underline{p}_{os} + \frac{M_f}{M_P}\underline{p}_f = \underline{p}_F \tag{17}$$

or

$$\alpha\underline{p}_{os} + (1-\alpha)\underline{p}_f = \underline{p}_F \tag{18}$$

with $\alpha = M_{os}/M_p$ and $1-\alpha = M_f/M_p$.

4.2. Mass balance around the ball mill

If we consider the general model for continuous ball milling operations, the dynamic mass balance on class i can be given by

$$\begin{array}{ccccccccc} M_F p_{Fi} & + & w\sum_{j=1}^{i-1} b_{ij}s_j p_{Lj} & = & d_i w p_{Li} & + & s_i w p_{Li} & + & \frac{d}{dt}(w p_{Li}) \\ \uparrow & & \uparrow & & \uparrow & & \uparrow & & \uparrow \\ \text{IN} & + & \text{PRODUCED} & = & \text{OUT} & + & \text{BROKEN} & + & \text{ACCUMULATED} \end{array} \tag{19}$$

and represents the in the ball mill.

The subscript L denotes the mill load.

Dividing both sides of Eq. (19) by M_F and using matrix notation, one gets

$$\underline{p}_F + \theta\underline{\underline{B}}\underline{\underline{S}}\underline{p}_L = \theta(\underline{\underline{D}} + \underline{\underline{S}})\underline{p}_L + \frac{d}{dt}(\theta\underline{p}_L) \tag{20}$$

with $\theta = W/F$ is the average residence time of the material in the mill, where $\underline{\underline{B}}$, $\underline{\underline{S}}$ and $\underline{\underline{D}}$ are breakage, selection and discharge matrices, respectively.

Assuming that the ball milling has reached steady state conditions, $d(\theta\underline{p}_L)/dt = 0$.

Solving for Eq. (20) gives

$$\underline{p}_L = \frac{1}{\theta}(\underline{\underline{D}} + \underline{\underline{S}} - \underline{\underline{B}}\underline{\underline{S}})^{-1}\underline{p}_F \tag{21}$$

Then

$$\underline{p}_P = \theta\underline{\underline{D}}\underline{p}_L = \underline{\underline{D}}(\underline{\underline{D}} + \underline{\underline{S}} - \underline{\underline{B}}\underline{\underline{S}})^{-1}\underline{p}_F \tag{22}$$

or

$$\underline{p}_P = \underline{\underline{T}}\underline{p}_F \tag{23}$$

where $\underline{\underline{T}}$ is the ball milling transformation matrix.

If the mill is assumed to be perfectly mixed and that there is not classification at the outlet ($P_P = P_L$), Eq. (19) becomes

$$p_{Fi} = p_{Pi} + \theta(S_i p_{Pi} - \sum_{j=1}^{i-1} S_j b_{ij} p_{Pj}) \tag{24}$$

Using the matrix notation, one gets

$$\underline{p}_F = \underline{p}_P + \theta(\underline{\underline{S}}\underline{p}_P - \underline{\underline{S}}\underline{\underline{B}}\underline{p}_P) \tag{25}$$

Finally

$$\underline{p}_P = \frac{\underline{p}_F}{\underline{\underline{I}} + \theta\underline{\underline{S}}(\underline{\underline{I}} - \underline{\underline{B}})} \tag{26}$$

4.3. Mass balance around the hydrocyclone

The mass balance written around the cyclone unit can be given by

$$M_o\underline{p}_o + M_u\underline{p}_u = M_P\underline{p}_P \tag{27}$$

Using the hydrocycloning transformation matrix $\underline{\underline{C}}$ one can get

$$M_u\underline{p}_u = \underline{\underline{C}}M_P\underline{p}_P \tag{28}$$

and

$$M_o\underline{p}_o = \left(\underline{\underline{I}} - \underline{\underline{C}}\right)M_P\underline{p}_P \tag{29}$$

4.4. Mass balance around the vibrating screen

The mass balance around the screen is given by

$$M_{os}\underline{p}_{os} + M_{us}\underline{p}_{us} = M_s\underline{p}_s \tag{30}$$

Using the screening transformation matrix $\underline{\underline{C}}^*$, one can get

$$M_{us}\underline{p}_{us} = \underline{\underline{C}}^* M_s \underline{p}_s \tag{31}$$

and

$$M_{os}\underline{p}_{os} = \left(\underline{\underline{I}} - \underline{\underline{C}}^*\right) M_s \underline{p}_s \tag{32}$$

The global model for the closed ball milling circuit can be given by

$$M_{us}\underline{p}_{us} = \underline{\underline{C}}^*\underline{\underline{C}}\left[\theta(\underline{\underline{D}} + \underline{\underline{S}} - \underline{\underline{BS}})\right]^{-1} M_F \underline{p}_F \tag{33}$$

or

$$M_{os}\underline{p}_{os} = \left(\underline{\underline{I}} - \underline{\underline{C}}^*\right)\underline{\underline{C}}\left[\theta(\underline{\underline{D}} + \underline{\underline{S}} - \underline{\underline{BS}})\right]^{-1} M_F \underline{p}_F \tag{34}$$

4.5. *Binary matrix representations*

The following matrices were used in this work. These matrices are of dimensions mn × mn, and it was assumed there is no interaction between the chromite (Cr) and non-chromite (NCr) components. It was also assumed that chromite and non-chromite were free particles.

$\underline{p}_F$ and $\underline{p}_P$ are vectors of dimensions mn × 1.

$$\underline{p}_F = \begin{bmatrix} p_{Cr1} \\ p_{Cr2} \\ \vdots \\ p_{Crm} \\ p_{NCr1} \\ \vdots \\ p_{NCrn} \end{bmatrix}_{mn\times 1} \quad \text{and} \quad \underline{p}_P = \begin{bmatrix} p_{Cr1} \\ p_{Cr2} \\ \vdots \\ p_{Crm} \\ p_{NCr1} \\ \vdots \\ p_{NCrn} \end{bmatrix}_{mn\times 1}$$

S is a diagonal matrix with diagonal elements S_{Cri}, i = 1, 2, …, m and S_{NCri}, i = 1, 2, …, *n*.

$$\underline{\underline{S}} = \begin{bmatrix} S_{Cr11} & 0 & 0 & 0 & 0 & 0 \\ \vdots & \ddots & \vdots & \vdots & \vdots & \vdots \\ 0 & 0 & S_{Crmm} & 0 & 0 & 0 \\ 0 & 0 & 0 & S_{NCr11} & 0 & 0 \\ \vdots & \vdots & \vdots & \vdots & \ddots & \vdots \\ 0 & 0 & 0 & 0 & 0 & S_{NCrnn} \end{bmatrix}_{mn\times mn}$$

B is a lower triangular matrix with elements b_{ij}, with $m,n \geq i > j \geq 1$.

$$\underline{\underline{B}} = \begin{bmatrix} 0 & 0 & \dots & 0 & 0 & 0 & 0 & \dots & 0 & 0 \\ b_{Cr21} & 0 & \dots & 0 & 0 & 0 & 0 & \dots & 0 & 0 \\ b_{Cr31} & b_{Cr32} & \dots & 0 & 0 & 0 & 0 & \dots & 0 & 0 \\ \dots & \dots & \dots & 0 & 0 & 0 & 0 & \dots & 0 & 0 \\ b_{Crm1} & b_{Crm2} & \dots & b_{Crmm-1} & 0 & 0 & 0 & \dots & 0 & 0 \\ 0 & 0 & \dots & 0 & 0 & b_{NCr21} & 0 & \dots & 0 & 0 \\ 0 & 0 & \dots & 0 & 0 & b_{NCr31} & b_{NCr32} & \dots & 0 & 0 \\ \dots & \dots & \dots & 0 & 0 & \dots & \dots & \dots & 0 & 0 \\ 0 & 0 & \dots & 0 & 0 & b_{NCrn1} & b_{NCrn2} & \dots & b_{NCrnn-1} & 0 \end{bmatrix}_{mn\times mn}$$

The discharge matrix can be represented as follows

$$\underline{\underline{D}} = \begin{bmatrix} D_{Cr11} & 0 & 0 & 0 & 0 & 0 \\ \vdots & \ddots & \vdots & \vdots & \vdots & \vdots \\ 0 & 0 & D_{Crmm} & 0 & 0 & 0 \\ 0 & 0 & 0 & D_{NCr11} & 0 & 0 \\ \vdots & \vdots & \vdots & \vdots & \ddots & \vdots \\ 0 & 0 & 0 & 0 & 0 & D_{NCrnn} \end{bmatrix}_{mn\times mn}$$

Similarly the cyclone partition curve matrix can be represented as follows

$$\underline{\underline{C}} = \begin{bmatrix} C_{Cr11} & 0 & 0 & 0 & 0 & 0 \\ \vdots & \ddots & \vdots & \vdots & \vdots & \vdots \\ 0 & 0 & C_{Crmm} & 0 & 0 & 0 \\ 0 & 0 & 0 & C_{NCr11} & 0 & 0 \\ \vdots & \vdots & \vdots & \vdots & \ddots & \vdots \\ 0 & 0 & 0 & 0 & 0 & C_{NCrnn} \end{bmatrix}_{mn\times mn}$$

Similarly the screen partition curve matrix can be represented by

$$\underline{\underline{C}}^* = \begin{bmatrix} C^*_{Cr11} & 0 & 0 & 0 & 0 & 0 \\ \vdots & \ddots & \vdots & \vdots & \vdots & \vdots \\ 0 & 0 & C^*_{Crmm} & 0 & 0 & 0 \\ 0 & 0 & 0 & C^*_{NCr11} & 0 & 0 \\ \vdots & \vdots & \vdots & \vdots & \ddots & \vdots \\ 0 & 0 & 0 & 0 & 0 & C^*_{NCrnn} \end{bmatrix}_{mn\times mn}$$

5. Experimental

5.1. *Description of the experimental laboratory mill*

An experimental laboratory scale ball mill designed and built at Mintek was used in this study. The ball mill measured 0.4 m in diameter and had four independent sections of 0.2 m each. It also allowed the use of variable liner types along the mill axial length. It was fitted with 12 lifters spaced circumferentially around the mill shell, with an average spacing-to-height

ratio (S/H) of ±0.6. It was driven by an asynchronous motor rated with power close to 10 kW. The optimum ball milling operating parameters, with respect to UG2 ores were determined by Kime [30] by using the Discrete Element Modelling (DEM) combined with milling testwork involving a UG2 ore sample.

5.2. The batch grinding test

Milling kinetics tests were conducted in order to quantify the individual milling kinetics of chromite and non-chromite during the ball milling of a UG2 ore sample. The one-size fraction method by Austin et al. [4] was used to determine the Breakage and Selection Function parameters. Four different monosize fractions were prepared and wet ground batch wise: −600 + 425 μm, −425 + 300 μm, −300 + 212 μm and, −212 + 150 μm. After the sample and the balls were loaded to the ball mill, it was run for 2 different time intervals (0.5 and 20 min). The short time provided data more strongly related to the Breakage Function for the ore, since not much secondary breakage was expected. The total individual composite samples for each test were carefully removed from the mill. They were weighed wet while still in the collection bucket, then pressure filtered, using tared filter papers before being placed on a pan and finally in an oven for drying over night at a temperature of about 65 °C. The dried samples were then re-weighed and a representative sample was taken for particle size distribution determination. Then, the feed for the next grinding period was the material retained on the screens, combined with the rest of the mill contents.

5.3. Simulation studies

The grinding circuit models Eq. (28)–(34) were simulated in Excel to explore the milling and classification options for UG2 ore. The sliming of chromite at flotation imposes that some constraints be taken during ball milling. The model parameters were determined based on the model predictions and were adjusted so as to minimize the chromite slimes (−38 μm) in the cyclone overflow stream, and to promote preferential grinding and preferential classification. The ball milling was assumed to be perfectly mixed. The Selection and Breakage Functions values of chromite and non-chromite components obtained from the batch ball milling tests were used to write the S and B matrices, along with the size and mineralogical composition of the feed. The Selection Function values were scaled up to a large mill (Mill throughput: 100 tons/h and Mill diameter: 4 m). In order to investigate the effects of improving the efficiency of the secondary circuit hydrocyclone, the hydrocyclone parameters were chosen as realistic as possible. Finally, the performance of the circuit including a hydrocyclone and closed by a screen with a 106 μm screen was investigated. The screen treated the hydrocyclone underflow. The screen oversized was recycled to the mill while the screen undersized was considered as a reject.

6. Results and discussion

6.1. Determination of the Selection Function

The graphical procedure of the full determination of all parameters associated with the Selection Function can be found in Austin et al. [4]. With respect to our data, the values of lambda (Λ) and gamma (γ) could not be determined. This is because all the feed sizes were not coarser. In other words, the breakage took place in the normal region (low-particle-size linear region, i.e. $S = ax^{alpha}$, where the media are large enough to break the particles efficiently. Therefore, the appropriate S values for abnormal breakage region were not described, as the maximum values for S were not reached. The magnitudes of the Selection Function for all feed sizes are shown in Fig. 2 for ball diameter = 20 mm, and Fig. 3 for ball diameter = 30 mm.

The values of a and alpha (α) in Eq. (4) are determined from Figs. 2 and 3 using a power function. The Selection

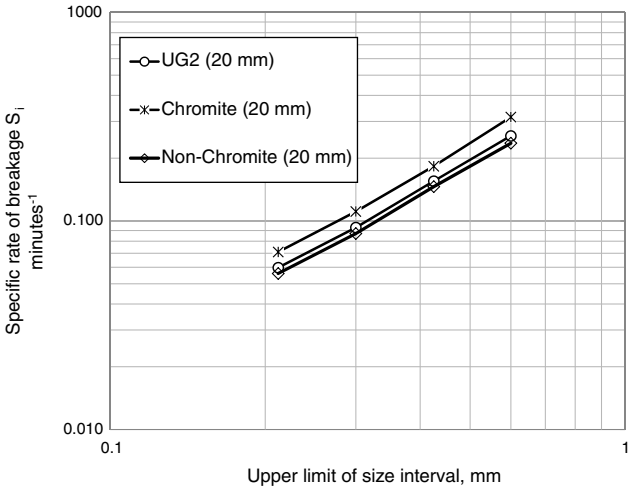

Fig. 2 – Specific rates of breakage of UG2 ore, chromite component and non-chromite component as a function of particle size (ball diameter = 20 mm).

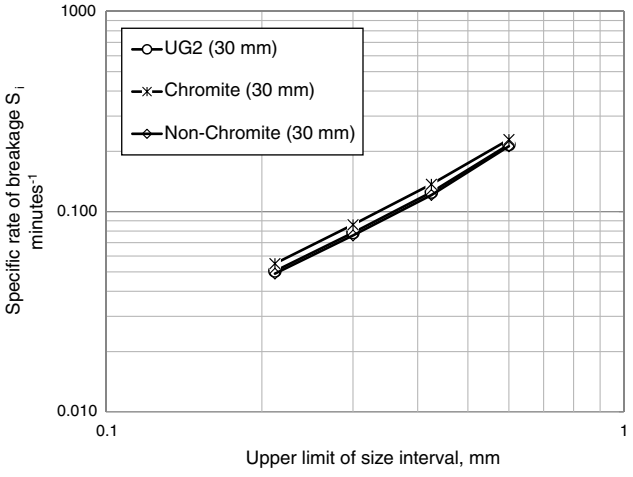

Fig. 3 – Specific rates of breakage of UG2 ore, chromite component and non-chromite component as a function of particle size (ball diameter = 30 mm).

Table 1 – Selection descriptive parameters.

Parameters	UG2 ore		Chromite component		Non-Chromite component	
Ball diameter	20 mm	30 mm	20 mm	30 mm	20 mm	30 mm
α	1.405	1.392	1.432	1.368	1.401	1.393
a	0.518	0.427	0.639	0.452	0.478	0.419

Table 2 – Breakage Function descriptive parameters.

Breakage Function parameters	UG2 ore		Chromite component		Non-chromite component	
Ball diameter	20 mm	30 mm	20 mm	30 mm	20 mm	30 mm
β	6.20	6.00	7.90	7.40	5.35	5.30
γ	1.34	1.30	1.14	1.05	1.22	1.16
Φ	0.62	0.60	0.75	0.71	0.56	0.55

Function parameters are summarized in Table 1. It can be seen that *a* and *alpha* values decreased with increasing ball diameters. This observation confirms the expected behaviour [31]. In all, it can be seen that high breakage rate (i.e. higher value of Si was obtained for chromite, whereas slow breakage rate was obtained for non-chromite. The breakage rate of the UG2 obtained ore was between the breakage rates of chromite and non-chromite components.

6.2. *Determination of the Breakage Function*

The B-II calculation procedure of the primary breakage function as proposed by Austin et al. [4] was used to generate the breakage function parameters. This method suggests use of shorter grinding times, which result in 20–30% broken materials out of the top size before re-breakage. Austin and Luckie [32] stated that up to 65% broken material will still provide accurate enough good data to be used with this procedure. The experimental values of cumulative breakage distribution function were fitted by Eq. (7), and the model parameters: β, γ and φ were then evaluated. All the feed materials were considered to be normalizable for simulation purposes. The average B_{ij} values obtained are illustrated in Fig. 4.

The average Breakage Function parameters are listed in Table 2. It can be seen that a low γ-value was obtained for chromite compared to non-chromite. This was an indication that chromite was a very soft material. It can also be seen that the γ-value was sensitive to the milling conditions, e.g. ball size. The results showed that γ decreased with an increase in the ball size dimensions. Conversely, higher values of Φ were obtained for the chromite compared to non-chromite, indicating that larger fraction of fine chromites were produced in a single fracture event.

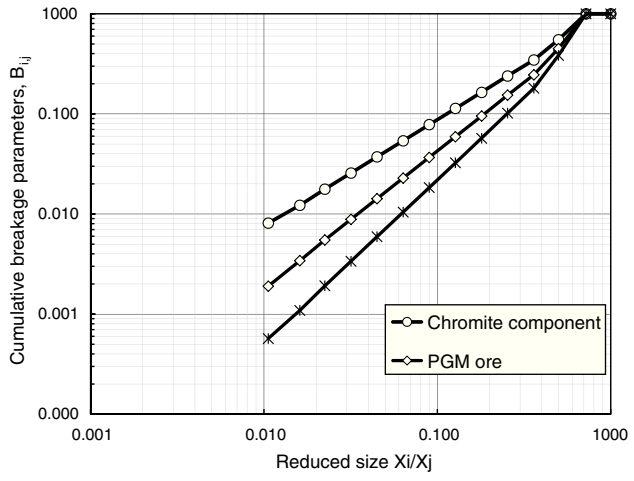

Fig. 4 – Comparison of the average primary breakage distributions.

6.3. *Grinding circuit model simulation results*

6.3.1. *Ball milling in closed circuit with a hydrocyclone*

In order to assess the effectiveness of the model developed, the ball milling in closed circuit with a hydrocyclone was considered. The grinding conditions were set so as to keep the offending chromite mineral more under control. The ball milling was simulated for a shorter period residence time $\theta = 12$ min. Optimistic parameter values were also set for the cyclone that was assumed operating efficiently. The sharpness of separation (m) and the bypass to the underflow (R_f) were assumed to be independent of the mineral type ($m = 1.61$ and $R_f = 15$ per cent). Only the cut sizes d^j_{50c} were assumed to vary with mineral type. The calculated chromite and non-chromite component cut-sizes obtained were 41.57 μm and 66.82 μm respectively, for $k_1 = 100$ (chosen arbitrarily to get reasonable values for the cut-sizes) and $k_2 = -0.5$. Fig. 5 shows the outcome of the simulation, with regard to the chromite and non-chromite size distribution in the final product streams. It can be seen that the percentage of the less than +106 μm in the hydrocyclone overflow has increased to 74.90% from 40.14% in the mill output. On the other hand, the percentage of the less than −38 μm chromite in cyclone overflow has increased to 41.50% from 9.81% in the mill output. This clearly highlights the challenge of operating the ball milling in closed circuit with a cyclone as large amount of fines is produced.

6.3.2. *Ball milling in closed circuit with a hydrocyclone and a vibrating screen*

Fig. 6 shows the effect of operating the secondary mill in closed circuit with a cyclone and a vibrating screen. The same operating parameters for the ball mill and cyclone were used as in the previous scenario. Realistic values were given for the screen parameters ($d^j_{50c} = 106$ μm, *alpha* = 2.4 and A = 95%). It can be seen that the amount of the less than +106 μm non-

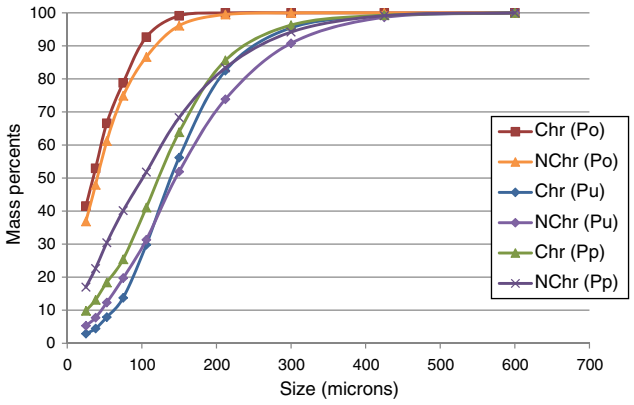

Fig. 5 – Total solids size distributions in the closed grinding circuit with a hydrocyclone.

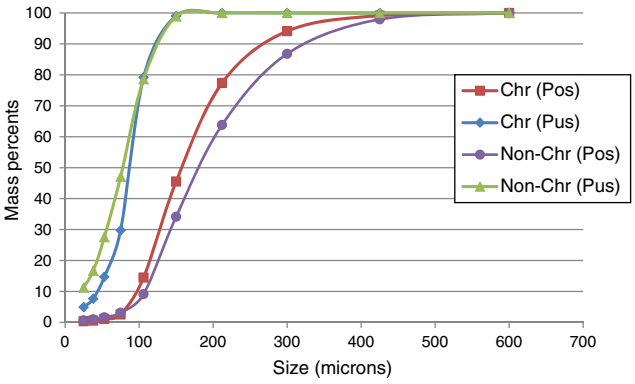

Fig. 7 – Solids size distributions around the vibrating screen.

chromite in the cyclone overflow has been increased to 74.46% from 46.96% in the mill output. At the same time the amount of the less than −38 μm chromite slimes has been increased to increased 33.88% from 9.80%. It can be seen that the effect of closing the circuit with a cyclone and screen has had only a marginal impact on the fineness of grind of the non-chromite. It should also be stressed that the configuration change has been done without significantly changing the circulating load or tonnage handled by the mill simulated. It can be seen that the percentage of the less than +106 μm of the non-chromite in the cyclone overflow has remain quasi unchanged. In other words, there is no advantage to be gained by operating the mill in closed circuit with a hydrocyclone and the screen at the same time if the objective of milling is to liberate PGMs in the non-chromites. However, the most noticeable gain in operating the mill in closed circuit with a cyclone and a screen is that the slimes content of the chromite in the cyclone overflow has reduced from 41.50% −38 μm to 33.88%. This means the incorporation of a screen in the grinding circuit to treat the cyclone underflow can substantially help reducing the chromite content in the cyclone overflow if large tonnages are processed at high re-circulating load.

Fig. 7 shows the size distributions in the screen products. For the cut-size set at +106 μm, it can be seen that most chromite slimes are prevented to be re-sent to the mill where they will be ground even finer and then report to the cyclone overflow. The screen undersize is therefore considered as a reject. It contains also some acceptable amount of non-chromite that can be compromised with the need to reduce the recirculation of fine chromites.

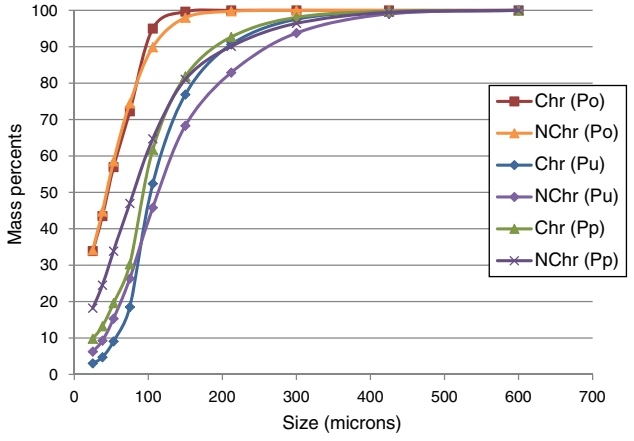

Fig. 6 – Total solids size distributions in the closed grinding circuit with a cyclone and a screen.

7. Conclusion

In this study, a binary matrix model of a closed circuit ball milling with a cyclone for the UG2 ore was presented. Conventionally these closed mill cyclone circuits operate with high circulating loads, between 200 and 400% and generally produce milled product at a specification of 80% less than 75 micron, which is required to liberate the PGMs. The problem comes largely with the Cr_2O_3, which is overmilled as the heavier Cr_2O_3 will continue to report to the cyclone underflow and returned to the mill. The results showed that by incorporating a screen in the circuit, the existing performance of the grinding circuits could be improved in terms of preferential grinding and classification for the non-chromite component within the UG2 ore. Screening the cyclone underflow will reduce significantly on a long run the amount of the chromite that reports to the cyclone overflow, while in the same time reducing high recirculation loads of chromite and therefore overmilling of chromite. However, in order to prove the viability of the model developed in this work, the findings obtained need to be backed by actual closed circuit continuous ball milling test work.

Conflicts of interest

The authors declare no conflicts of interest.

Acknowledgement

The authors acknowledge the financial support from the Council for Mineral Technology (Mintek) for this research work.

REFERENCES

[1] Lynch AJ. Mineral crushing and grinding circuits, their simulation, optimization, design and control. Amsterdam: Elsevier Scientific Publishing Co.; 1977. p. 340.

[2] Napier-Munn TJ, Morrell S, Morrison RD, Kojovic T. Mineral comminution circuits – their operation and optimization. JKMRC monograph series University of Queensland; 1996, 413 pp.

[3] Yekeler M. Breakage and morphological parameters determined by laboratory tests. Handbook of powder technology, vol. 12; 2007. p. 437–86 [Chapter 9]. ISSN: 0167-3785.

[4] Austin LG, Klimpel RR, Luckie PT. Process engineering of size reduction: ball milling. New York: Society of Mining Engineers of the AIME; 1984.

[5] Finch AJ, Ramirez Castro J. Modelling of mineral size reduction in the closed circuit ball mill at the Pine Point Mines concentrator. Int J Miner Process 1981;7:1–31.

[6] Laplante AR, Finch J, del-Villar R. Simplification of grinding equation for plant simulation. Trans Inst Miner Metall (Lond) Sect C 1987;96(June):C108–12.

[7] Morrell S. A new autogenous and semi-autogenous mill model for scale-up, design and optimisation. Miner Eng 2004;17(3):437–45.

[8] Hinde AL, Kalala JT. The application of a simplified approach to modelling tumbling mills, stirred media mills and HPGRs. Miner Eng 2009;22:633–41.

[9] Powell MS, Morrison RD. The future of comminution modelling. Int J Miner Process 2007;84(1–4):228–9.

[10] Choi WZ, Adel GT, Yoon RH. Estimation of model parameters for liberation and size reduction. Miner Metall Process 1988:33–9.

[11] Herbst JA, Rajamani K, Lin CL, Miller JD. Development of a multicomponent-multisize liberation model of a grinding-liberation model. Miner Eng 1998;1(2):97–111.

[12] Mailula T, Bradshaw D, Harris P. The effect of copper sulphate addition on the recovery of chromite in the flotation of UG2 ore. S Afr Inst Min Metall 2003;103(2): 143.

[13] Hay MP. A case study of optimising UG-2 flotation performance part 2: modelling improved PGM recovery and Cr_2O_3 rejection at Northam's UG-2 concentrator. Miner Eng 2010;23:868–76.

[14] Hay MP, Roy R. A case study of optimising UG-2 flotation performance, part 1: bench, pilot and plant scale factors which influence Cr_2O_3 entrainment in UG-2 flotation. Miner Eng 2010;23:855–67.

[15] Mckenzie A. The presence of spinel during matte smelting. In: Proc. trends in base metal smelting and refining. 1996.

[16] Penberthy CO. The recovery of platinum group elements from the UG-2 chromite, Bushveld Complex – a mineralogical perspective. Mineral Petrol 2000;68:213–22.

[17] Hay MP, Schroeder G. Use of the SUPASIM flotation model in optimizing Impala's UG2 circuit. Miner Eng 2005;18:772–84.

[18] Liddell K. 25 years of UG2 concentrators. In: A celebration of technology conference. Mintek 75'. 2009.

[19] Becker M, Mainza AN, Powell MS, Bradshaw DJ, Knopjes B. Quantifying the influence of classification with the 3 product cyclone on liberation and recovery of PGEs in UG2 ore. Miner Eng 2008;21:549–58.

[20] Schumann R. Energy input and size distribution in comminution. Trans AIME 1960;217:22–5.

[21] Lynch AJ, Whiten WJ, Narayanan SS. Ball mill models: their evolution and present status. In: Arbiter symposium. 1986. p. 48–66.

[22] Austin LG. Rate equations for non-linear breakage in mills due to materials effects. Powder Technol 1982:127–33.

[23] Gardner RP. A two mechanistic approach for the comminution of material that exhibits heterogeneous breakage characteristics. Powder Technol 1975;12:247–58.

[24] Austin LG, Brame K. A comparison of Bond method for sizing wet tumbling ball mills with a size-mass balance simulation model. Powder Technol 1983;34(2):261–74.

[25] Tangsathitkulchai C. Effects of slurry concentration and powder filling on the net power of a laboratory ball mill. Powder Technol 2003;137(3):131–8.

[26] Plitt LR. A mathematical model for the hydrocyclone classifier. CIM Bull 1976;69:114.

[27] Rogers RSC. A classification function for vibrating screens. Powder Technol 1982;31(1):135–7.

[28] Modrzewski R, Wodzinski P. Screens for segregation of mineral waste. Physicochem Probl Miner Process 2011;47:267–74.

[29] Bilgili E, Yepes J, Scarlett B. Formulation of a non-linear framework for population balance modeling of batch grinding: beyond first-order kinetics. Chem Eng Sci 2006;61(1):33–44.

[30] Kime MB. Using the discrete-element method to investigate ball milling power draw, load behaviour, and impact energy profile. Can Inst. Min. Metall. Pet. J 2017;8(1), http://dx.doi.org/10.15834/cimj.2017.3.

[31] Austin LG, Shoji K, Luckie PT. The effect of ball size on mill performance. Powder Technol 1976;14(1):71–9.

[32] Austin LG, Luckie PT. The estimation of non-normalized breakage distribution parameters from batch grinding tests. Powder Technol 1972;5(5):215–22.